Intelligent adaptive model for the helicopter turboshaft engines' gas temperature sensor readings correction

Serhii Vladov[1,*,†], Victoria Vysotska[2,†], Vasyl Lytvyn[2,†], Yelyzaveta Sahun[3,†], Nataliia Vladova[3,†], and Mykhailo Luchkevych[2,†]

[1] *Kharkiv National University of Internal Affairs, L. Landau Avenue 27 61080 Kharkiv, Ukraine*
[2] *Lviv Polytechnic National University, Stepan Bandera Street 12 79013 Lviv, Ukraine*
[3] *Ukrainian State Flight Academy, Chobanu Stepana Street 1 25005 Kropyvnytskyi, Ukraine*

Abstract

The article develops an intelligent adaptive model for correcting the helicopter turboshaft engine gas temperature in front of the compressor turbine sensor readings, based on a hybrid variational-Bayesian MLP network with two hidden layers and Smooth ReLU activation. The model combines a physical-statistical component, a first-order dynamic error, the calibration drift approximation by a sensor time polynomial, a nonlinear characteristic expanded in a Taylor series up to the third order, and machine learning methods: the recursive least squares (RLS) method for initialising parameters and Bayes by Backprop for estimating the weight distribution uncertainty. The variational approximation μ and Σ is initialised based on the RLS results, which ensures fast convergence and regularisation of training based on physical assumptions. The experimental validation was performed in MATLAB Simulink 2014b using real flight data of the TV3-117 engine on the Mi-8MTV helicopter (clock step 0.25 seconds, total time 320 seconds, maximum temperature 1140 K). The results showed that the third-order nonlinear characteristic approximation provides an error of no more than 0.1 K within 1080–1150 K, and the RLS estimates for the drift parameters and dynamics τ and α reach 50% convergence in the first 20 steps. With variational training, ELBO increased from −440 to −45 in 100 epochs and stabilised by the 50th iteration. The developed model demonstrated high indicators: Accuracy = 0.992; recall = 0.997; precision = 0.988; F1-score = 0.987; average training time is about 182 seconds with an accuracy variance of about $1.08 \cdot 10^{-6}$. Comparative analysis with 1D-CNN, LSTM/GRU, and extended Kalman filter confirmed the developed model's improvement in terms of resistance to noise and sensor drift in real time up to 5%.

Keywords

Adaptive sensor correction, variational Bayesian MLP network, recursive least squares (RLS), polynomial calibration drift, Taylor approximation of nonlinear characteristic, helicopter turboshaft engine

1. Introduction

The development of the modern helicopter turboshaft engine (TE) requires precise control of its operating parameters [1], among which is the gas temperature in front of the compressor turbine [2, 3]. Gas temperature sensor readings are influenced by external factors (ambient temperature fluctuations, vibrations, carbon formation on the sensitive element), as well as the sensor itself ageing and errors in the measuring equipment [4]. As a result, the accumulation of errors can lead to the engine thermal mode estimates' distortion, which reduces operating efficiency, increases fuel

PhD Workshop on Artificial Intelligence in Computer Science at 9th International Conference on Computational Linguistics and Intelligent Systems (CoLInS-2025), May 15–16, 2025, Kharkiv, Ukraine

⋆ You should use this document as the template for preparing your publication. We recommend using the latest version of the CEURART style.

* Corresponding author.
† These authors contributed equally.
serhii.vladov@univd.edu.ua (S. Vladov); victoria.a.vysotska@lpnu.ua (V. Vysotska); vasyl.v.lytvyn@lpnu.ua (V. Lytvyn); nataliia.vladova@sfa.org.ua (N. Vladova); yelyzavetasahun@sfa.org.ua (Y. Sahun); mykhailo.m.luchkevych@lpnu.ua (M. Luchkevych)
0000-0001-8009-5254 (S. Vladov); 0000-0001-6417-3689 (V. Vysotska); 0000-0002-9676-0180 (V. Lytvyn); 0000-0003-4837-4688 (Y. Sahun); 0009-0009-7957-7497 (N. Vladova); 0000-0002-2196-252X (M. Luchkevych)

consumption, and provokes the components' premature wear. The introduction of the intelligent adaptive correction model [5, 6] helps quickly find and fix both regular and random measurement errors, ensuring accurate control in real time.

The research relevance is due to the growing requirements for helicopter flight reliability and safety [7, 8] in intensive operation and various climatic zone conditions. An intelligent model based on machine learning methods [9, 10] and Bayesian algorithms [11, 12] will be able to adapt to changing engine operating conditions, adjusting sensor readings without the need for frequent calibration or equipment replacement. It will ensure a significant increase in the helicopter TE service life, reduce operating costs for maintenance, and improve flight safety due to more accurate prediction of thermal loads and emergency mode prevention.

2. Related works

Existing methods for compensating errors in helicopter TE temperature sensors [13–15] traditionally rely on strictly specified correction characteristics and periodic calibration. Classical approaches include the sensor response dependence linear [16, 17] and polynomial [18, 19] models based on the proper temperature, where laboratory tests determine the coefficients. However, the models developed in [16–19] are poorly adapted to changes in external flight conditions and do not take into account the measurement circuit elements' ageing effect, which leads to systematic errors over time.

In recent years, adaptive filters have become widespread, in particular the Kalman filter [20] and its extended modifications [21–24], used to estimate the engine's actual thermal state based on data from several sensors. These methods demonstrate high accuracy in the presence of a correct mathematical model of the process dynamics. Still, they are sensitive to incorrect initialisation of covariance matrices and require significant computational resources when processing multidimensional vector states in real time.

Machine learning (ML) methods have begun to be implemented for the analysis of large datasets obtained during the helicopter TE ground and flight tests [25–28]. In the last decade, researchers, for example, in [29–32], have proposed neural network correlators [29, 30] that are capable of training sensors with nonlinear characteristics without explicitly specifying a physical model, as well as models based on gradient boosting [31, 32] for predicting correction values. However, such solutions are often "black box" [33] and do not provide a transparent understanding of the error causes. They can also be retrained in specific modes, losing accuracy when moving to new conditions.

Bayesian calibration methods [11, 12, 34, 35] represent an elegant compromise between a rigid physical model and the ML approaches' flexibility: they allow one to introduce a priori information about the sensor behaviour and update the model parameters' estimates as new data arrive. In particular, Gibbs Markov chains [36] and variational Bayesian approximations [37] have been used to estimate random and systematic deviations in readings. The problem remains highly computationally complex, with an increase in the number of parameters and the need for well-founded a priori distributions.

Hybrid solutions at the Bayesian and ML models junction propose using neural networks [38, 39] to set the correction functional form and to train the parameters using the variational Bayes method. Such approaches demonstrate better results in the incomplete data conditions and allow one to estimate the correction signal uncertainty. However, the studies are still limited to laboratory data, and the algorithms' scalability issues for integration into onboard computing systems remain open.

In the helicopter TE sensors failure diagnostics and residual life prediction field, methods for detecting anomalies in the measurement stream are being actively developed [40–44]. Algorithms based on autoencoders [40] and LSTM networks [41] allow detecting sharp and hidden "chatter" in readings associated with mechanical damage or electrical failures. However, most existing studies, including [42–44], focus on classifying failures that have already occurred, rather than on continuous data correction in real time to prevent error accumulation.

The following key issues remain unresolved, requiring the intelligent adaptive correction model development:

1. Continuous online calibration should be provided, taking into account ageing, contamination, and vibration effects without taking the sensor service out.
2. Adaptation to rapidly changing thermal flight conditions with minimal computational delays and limited resources of onboard computers.
3. Reasonable unification of helicopter TE dynamics physical models with flexible ML structures and Bayesian uncertainty processing.
4. Development of methods for assessing the confidence in corrected readings and automatic transition to emergency mode when parameters go beyond safe limits.

The solution to these problems will make it possible to create a reliable intelligent system for correcting sensory data, which will significantly increase the helicopter's TE thermal state monitoring accuracy.

3. Materials and methods

3.1. Development of an adaptive model for correcting temperature sensor readings

Based on [9, 20, 24, 29, 33, 40], $T_G^{*(true)}(t)$ it is set that is the actual gas temperature in front of the compressor turbine at the measurement point; $T_G^{*(meas)}(t)$ is the temperature sensor reading; $\Delta_{dyn}(t)$ is the error due to dynamic load changes; $\Delta_{drift}(t)$ is the calibration (aging) drift; $\varepsilon(t)$ is the random noise component. Then the general model is represented as:

$$T_G^{*(meas)}(t) = T_G^{*(true)}(t) + \Delta_{dyn}(t) + \Delta_{drift}(t) + \varepsilon(t). \quad (1)$$

The dynamic error model creates, it is assumed that the dynamic component depends on the temperature change rate and load $u(t)$ [6, 7], described by a first-order differential equation in the form:

$$\Delta_{dyn}(t) = \tau \cdot \frac{dT_G^{*(meas)}}{dt} + \alpha \cdot u(t), \quad (2)$$

where τ is the sensor's temporary setting and α is the sensitivity to external load.

Substituting (2) into (1) yields:

$$T_G^{*(meas)}(t) = T_G^{*(true)}(t) + \tau \cdot \frac{dT_G^{*(meas)}}{dt} + \alpha \cdot u(t) + \Delta_{drift}(t) + \varepsilon(t). \quad (3)$$

It is assumed that the drift $\Delta_{drift}(t)$ changes slowly and can be approximated by a time polynomial of the form:

$$\Delta_{drift}(t) \approx \sum_{k=0}^{N} b_k \cdot t^k, \quad (4)$$

which allows adaptive estimation of the coefficients b_k.

Often the temperature sensor has a nonlinear characteristic $f(\bullet)$ [9, 16–20, 24, 29, 33, 40], so that

$$T_G^{*(meas)} = f\left(T_G^{*(true)}\right) + \tau \cdot \frac{dT_G^{*(meas)}}{dt} + \alpha \cdot u(t) + \sum_{k=0}^{N} b_k \cdot t^k + \varepsilon(t), \quad (5)$$

Let us expand f into a Taylor series around the operating point T_0:

$$f(T) = f(T_0) + f'(T_0) \cdot (T - T_0) + \frac{f''(T_0)}{2!} \cdot (T - T_0)^2 + \ldots + \frac{f^{(M)}(T_0)}{M!} \cdot (T - T_0)^M + R_{M+1}, \quad (6)$$

where R_{M+1} is the remainder term.

Introducing the notation $\Delta T = T_G^{*(true)} - T_0$, we obtain

$$f\left(T_G^{*(true)}\right) \approx \sum_{k=0}^{M} a_i \cdot \left(\Delta T\right)^i, \quad a_i = \frac{f^{(i)}\left(T_0\right)}{i!}. \tag{7}$$

Substituting (7) into (3), we obtain:

$$T_G^{*(meas)} \approx \sum_{k=0}^{M} a_i \cdot \left(\Delta T\right)^i + \tau \cdot \frac{dT_G^{*(meas)}}{dt} + \alpha \cdot u\left(t\right) + \sum_{k=0}^{N} b_k \cdot t^k + \varepsilon\left(t\right), \tag{8}$$

For $T_G^{*(true)}$ restoration, a correction function $\hat{E}(\square)$ is determined:

$$\hat{E}\left(T_G^{*(meas)}, u, t\right) \approx \sum_{k=0}^{M} \hat{a}_i \cdot \left(T_G^{*(meas)} - T_0\right)^i + \sum_{k=0}^{N} \hat{b}_k \cdot t^k + \hat{\tau} \cdot \frac{dT_G^{*(meas)}}{dt} + \hat{\alpha} \cdot u\left(t\right), \tag{9}$$

Then the assessment is defined as:

$$T_G^{*(true)} = T_G^{*(meas)} - \hat{E}\left(T_G^{*(meas)}, u, t\right), \tag{10}$$

For the adaptive parameter estimation purposes, it is assumed that a parameter vector of the form is formed:

$$\boldsymbol{\theta} = \left[\hat{a}_0, \hat{a}_1, ..., \hat{a}_M, \hat{b}_0, ..., \hat{b}_N, \hat{\tau}, \hat{\alpha}\right]^T, \tag{11}$$

and the input regressor vector has the form:

$$\boldsymbol{\phi}\left(t\right) = \left[1, \left(T_G^{*(meas)} - T_0\right), ..., \left(T_G^{*(meas)} - T_0\right)^M, t^0, ..., t^N, \dot{T}_G^{*(meas)}, u\left(t\right)\right]^T, \tag{12}$$

Then model (10) can be rewritten linearly in terms of parameters:

$$\hat{T}_G^{*(true)} = T_G^{*(meas)} - \boldsymbol{\phi}^T\left(t\right) \cdot \boldsymbol{\theta}, \tag{13}$$

Let the reference temperature $T_G^{*(ref)}$ be measured (from the reference device), then the error is defined as:

$$\varepsilon\left(t\right) = T_G^{*(ref)}\left(t\right) - \hat{T}_G^{*(true)}\left(t\right), \tag{14}$$

For adaptive parameter estimation, the recursive least squares (RLS) method is used:

$$\begin{gathered} K\left(t\right) = \frac{\boldsymbol{P}\left(t-1\right) \cdot \boldsymbol{\phi}\left(t\right)}{\lambda \cdot \boldsymbol{\phi}^T\left(t\right) \cdot \boldsymbol{P}\left(t-1\right) \cdot \boldsymbol{\phi}\left(t\right)}, \\ \boldsymbol{\theta}\left(t\right) = \boldsymbol{\theta}\left(t-1\right) + \boldsymbol{K}\left(t\right) \cdot e\left(t\right), \\ \boldsymbol{P}\left(t\right) = \frac{1}{\lambda} \cdot \left[\boldsymbol{I} - \boldsymbol{K}\left(t\right) \cdot \boldsymbol{\phi}^T\left(t\right)\right] \cdot \boldsymbol{P}\left(t-1\right), \end{gathered} \tag{15}$$

where $\lambda \in (0, 1]$ is the "forgetting" factor, P is the covariance matrix.

The developed adaptive model combines a dynamic part (time constant), calibration drift (time polynomial), and a nonlinear characteristic (Taylor series). The recursive least squares method provides automatic updating of parameters during operation, which allows the helicopter TE gas temperature to be reduced in front of the compressor turbine measurement error.

The sensor characteristic function expansion in a Taylor series around the operating point T_0 allows us to approximate an arbitrary smooth nonlinear dependence $f(T)$ by a polynomial with a controlled order, which simplifies the model structure (linearisation by parameters) and applies efficient adaptive algorithms (e.g., RLS); the polynomial approximation of the calibration drift over time $\sum b_k \cdot t^k$ reflects long-term changes in the sensor sensitivity; the R_{M+1} series residual term provides the approximation uncertainty analytical estimate, which allows us to balance between accuracy and computational complexity; and error control within the operating temperature region will enable us to select the series optimal order to minimise measurement errors.

3.2. Development of an adaptive model for correcting temperature sensor readings

In order to automatically correct the helicopter TE temperature sensor readings under changing operating conditions, a neural network architecture (Figure 1) is proposed, implementing a hybrid adaptive model for fixing the helicopter TE temperature sensor readings based on the developed model components: the basic measurement model (1), the dynamic component (2), the calibration drift (4), and the sensor nonlinear characteristic approximation by the Taylor series (6).

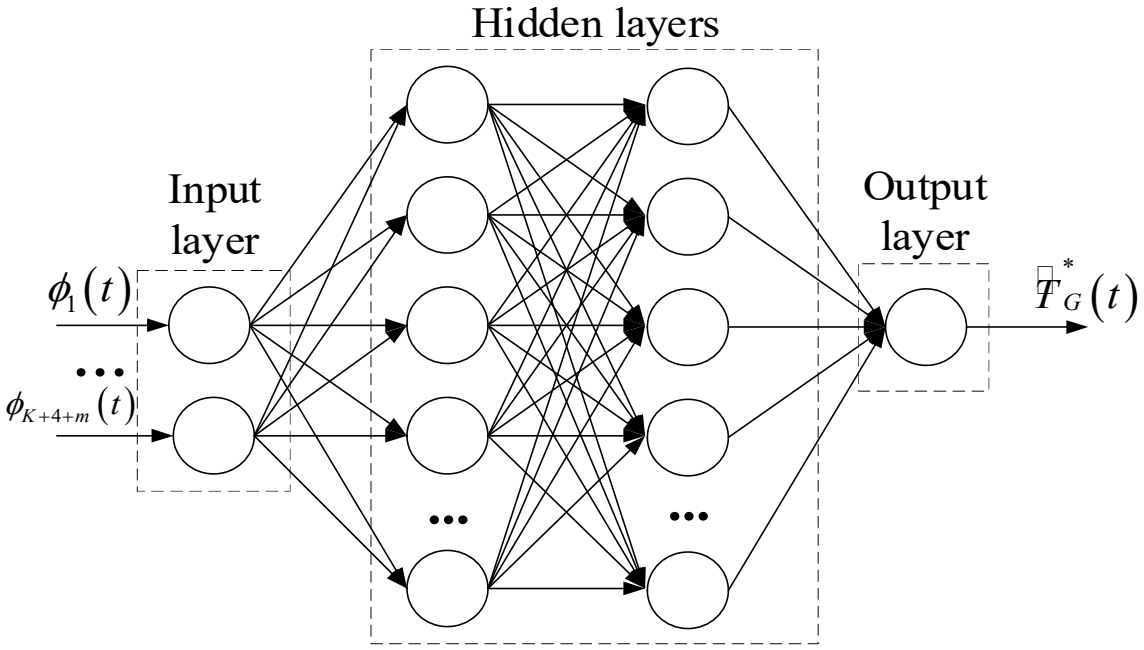

Figure 1: The developed neural network architecture. (author's research).

The neural network (Figure 1) input features are: $\phi_1(t) = y(t)$, $\phi_2(t) = \frac{dy(t)}{dt}$, (approximation, for example, by a moving average), $\phi_3(t) = u(t)$, $\phi_{3+k}(t) = t^k$, k = 0, 1, ..., K, $\phi_{3+k}(t) = t^k$, $\phi_{K+4+m}(t) = \left(y(t) - T_0\right)^m$, m = 0, 1, ..., M.

Then the general feature vector (11) takes the form:

$$\phi(t) = \left(\phi_1, \phi_2, \phi_3, \phi_4, ..., \phi_{K+4}, \phi_{K+5}, ..., \phi_{K+M+5}\right)^{\mathrm{T}}. \quad (16)$$

The neural network architecture contains an input layer of dimension $D = 3 + (K + 1) + (M + 1)$, two hidden layers of size H with the Smooth ReLU activation function [45, 46], and an output layer without activation, giving the adjusted value:

$$\hat{T}_G^*(t) = y(t) - \hat{\Delta}(t;\theta), \tag{17}$$

where

$$\hat{\Delta}(t;\theta) = NN(\phi(t);\theta), \tag{18}$$

where θ is the neural network parameter.

A variational Bayesian approach is used to take into account the neural network parameter uncertainties. For this aim, an a priori distribution of the form is introduced:

$$p(\theta) \sim N(0, \sigma_0^2 I), \tag{19}$$

and a variational approximation is selected:

$$q(\theta;\mu,\Sigma) = N(\mu,\Sigma). \tag{20}$$

Then, training the neural network is reduced to minimising the negative ELBO (evidence lower bound) [11, 12, 24, 47]:

$$L(\mu,\Sigma) = \mathrm{KL}\left(q(\theta;\mu,\Sigma)\middle\|p(\theta)\right) - E_{q(\theta;\mu,\Sigma)}\left[\log\left(p(D|\theta)\right)\right], \tag{21}$$

where is the dataset $D = \left\{\phi(t_i), T_G^{*(ref)}(t_i)\right\}_{i=1}^N$, and the likelihood is given by:

$$p(D|\theta) = \prod_{i=1}^N N\left(T_G^{*(ref)}(t_i)\middle|y(t_i) - NN(\phi(t_i);\theta), \sigma^2\right). \tag{22}$$

The gradients with respect to μ and Σ are calculated using Bayes by Backprop and updated using stochastic gradient descent [48]:

$$\frac{\partial L}{\partial \mu} = \Sigma^{-1}(\mu - 0) - \mathrm{E}_{q(\theta)}\left[\nabla_\theta \log\left(p(D|\theta)\right)\right],$$

$$\frac{\partial L}{\partial \Sigma} = \frac{1}{2}\cdot\left(\Sigma^{-1} - \Sigma^{-1}\cdot \mathrm{E}_{q(\theta)}\left[(\theta-\mu)\cdot(\theta-\mu)^{\mathrm{T}}\right]\cdot\Sigma^{-1}\right), \tag{23}$$

$$\mu \leftarrow \mu - \eta\cdot\frac{\partial L}{\partial \mu},\ \ \Sigma \leftarrow \Sigma - \eta\cdot\frac{\partial L}{\partial \Sigma},$$

where

$$\nabla_\theta \log\left(p(D|\theta)\right) = \sum_{i=1}^N \frac{T_G^{*(ref)}(t_i) - \left(y(t_i) - NN(\phi(t_i);\theta)\right)}{\sigma^2}, \tag{24}$$

where the parameters θ are estimated by the recursive least squares (RLS) method according to (15), and the prediction error is defined as

$$\varepsilon(t) = T_G^{*(ref)}(t) - \left(y(t) - \theta^{\mathrm{T}}\cdot\phi(t)\right). \tag{25}$$

In the developed hybrid model, the RLS method is used as an effective way to estimate the neural network parameters initially. Specifically, the $\theta^{(0)}$ and the covariance matrix $P^{(0)}$ values obtained from RLS according to (15) are used to initialise the variational approximation parameters $\mu = \theta^{(0)}$, $\Sigma = P^{(0)}$. The proposed approach accelerates the training and provides convergence of the neural network a priori regularisation based on physical assumptions and the linear structure of error.

4. Results

4.1. The experimental setup description

In this research, a computational experiment was carried out based on the developed adaptive model implementation for correcting the helicopter TE gas temperature in front of the compressor turbine sensor readings in the MATLAB Simulink 2014b environment (Figure 2).

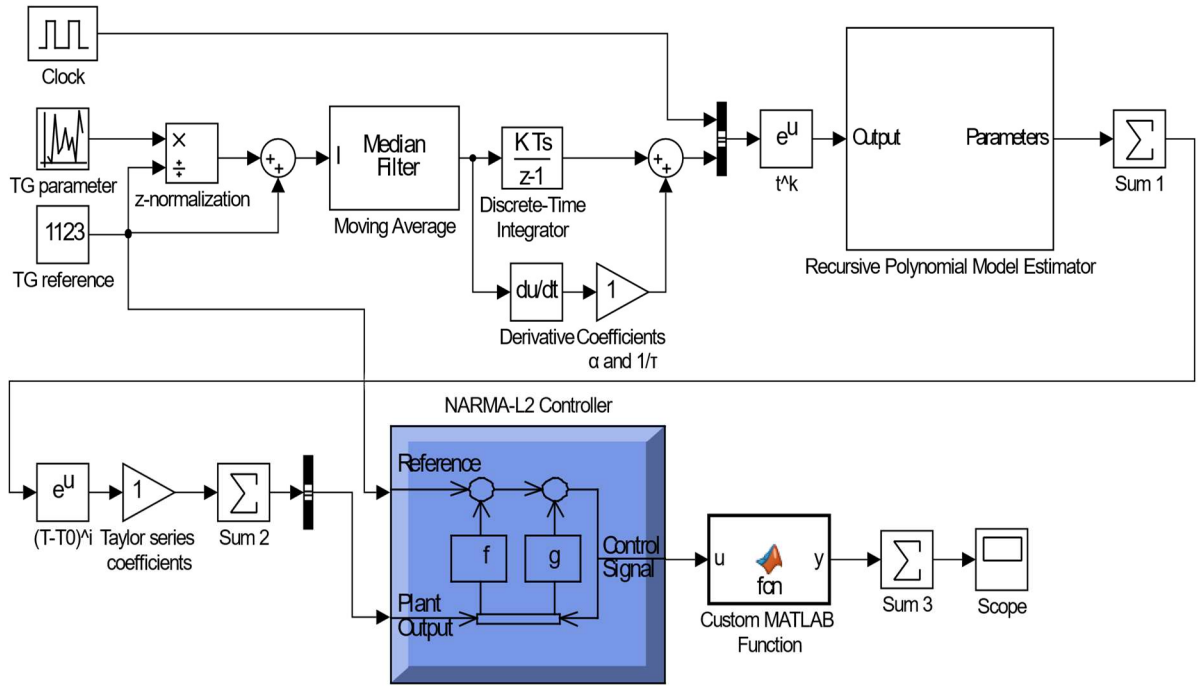

Figure 2: Experimental model diagram in MATLAB Simulink 2014b environment (author's research).

The "Signals Preprocessing" subsystem receives raw readings from the temperature sensor $T_{raw}(t)$ and normalises and smooths them before feeding them to the model further stages: first, z-normalization is performed through the Z-normalization and Sum blocks $\bar{T} = \frac{T_{raw} - \mu}{\sigma}$, the signal is then passed through a moving average filter to remove high frequency noise and produce a smoothed value $\overline{T}$; both signals received are normalised $\bar{T}$ and smoothed $\overline{T}$ are output and then distributed to the dynamic error and polynomial drift subsystems, providing a single scale of input data and preliminary filtering of noise components.

The "Dynamic Error" subsystem receives a normalised value $\bar{T}$ as input and evaluates its rate of change through the "Derivative block" $u = \frac{d\bar{T}}{dt}$, after which the coefficient α is applied using "Gain" and the signal is sent to the "Discrete-Time Integrator", which implements the dynamics $\tau \cdot \frac{d\Delta_{dyn}}{dt} + \Delta_{dyn} = \alpha \cdot u(t)$, the final value $\Delta_{dyn}(t)$ is formed by the "Sum" block, which sums the integrator output and the weighted signal, and is then transferred to the neural network regressor vector, taking into account the sensor response inertial properties and time delay.

The "Polynomial Drift" subsystem tracks the slow drift of sensor readings using a polynomial calibration model: the "Clock" block generates the current time t, after which the basis vectors t^k for k = 0...M are calculated via the "Math Function" and "Gain" chain, then the "MATLAB Function" recursively updates the least squares method coefficients b_k, and the Sum block generates the final

drift value $\Delta_{drift}(t) = \sum_{k=0}^{M} b_k \cdot t^k$, which is fed into the neural network regressor vector to compensate for long-term calibration changes.

The subsystem "The nonlinear characteristic approximation" takes a normalised value $\tilde{T}$ and through Math Function blocks sequentially calculates powers $\left(\tilde{T} - T_0\right)^i$ for i = 1...N, then each term is multiplied by the corresponding Taylor series coefficient ai by the "Gain" block, after which the "Sum" block sums all the terms up to a given order N, forming an approximate nonlinear value $f_{Taylor}\left(\tilde{T}\right)$, which is then fed into the neural network input vector to take into account the sensor physical characteristics.

The "Variational Bayesian MLP" subsystem generates an input regressor vector via the "Bus Creator" block, combining $\tilde{T}$, $\overline{T}$, Δ_{dyn}, Δ_{drift} and f_{Taylor}. The μ and Σ parameters initial estimates obtained from RLS are loaded into the "MATLAB Function", after which the signal passes two Fully Connected layers with SmoothReLU (Narma L2-controller) activation, and the "Custom MATLAB Function" block performs a variational Bayesian training step (Bayes by Backprop), updating μ and Σ using ELBO gradients; the neural network output y_{NN} is subtracted from the original T_{raw} via "Sum", generating a corrected value T_{corr}, which is simultaneously transferred to "Scope" for logging and evaluating quality metrics.

4.2. The input data analysis and preprocessing

To conduct the computational experiment, the TV3-117 engine gas temperature in front of the compressor turbine data were used, recorded in the Mi-8MTV helicopter flight mode by a standard sensor consisting of 14 dual thermocouples T-102 in the nominal engine operating mode [9, 20, 24, 29, 33, 40, 45, 46, 49]. The experiments were conducted under conditions when the altitude above sea level reached 2500 meters. Measurements were made for 320 seconds with data recording every 0.25 seconds. According to the data shown in Figure 3, the gas temperature in front of the compressor turbine's maximum value was 1140 K.

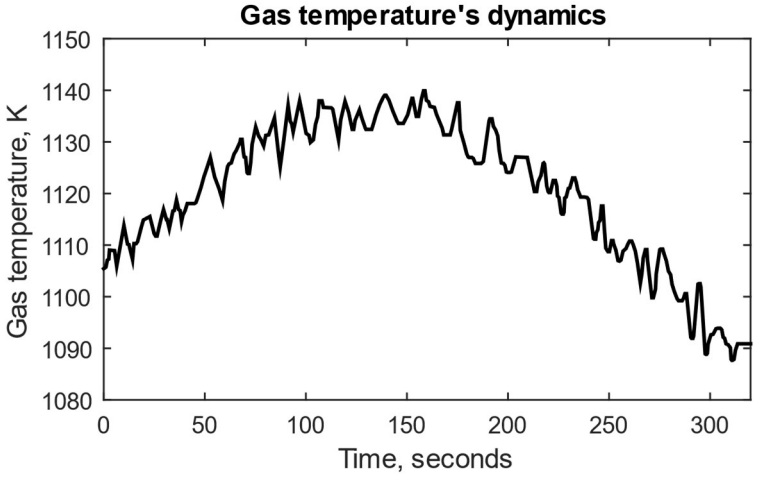

Figure 3: The gas temperature in front of the compressor turbine output signal diagram (author's research).

The gas temperature in front of the compressor turbine's T_G^* initial measurements, obtained during the Mi-8MTV helicopter flight tests using the onboard monitoring system, were preliminarily cleared of noise interference and abnormal emissions. Then these data were transformed into a time series, and the parameter sequences were ordered by time [50]. To bring time series of different scales to a comparable form, the z-normalisation procedure was applied:

$$z\left(T_G^*\right)_i = \frac{T_G^{*(i)} - \frac{1}{N}\cdot\sum_{i=1}^{N} T_G^{*(i)}}{\frac{1}{N}\cdot\sum_{i=1}^{N}\left(T_G^{*(i)} - \frac{1}{N}\cdot\sum_{i=1}^{N} T_G^{*(i)}\right)^2}. \quad (26)$$

where $N = 4 \cdot 320 = 1280$.

The gas temperature in front of the compressor turbine T_G^* and normalised values formed a training sample, which is given in Table 1. It is noted that this sample meets the homogeneity requirements according to the Fisher–Pearson [51, 52] and Fisher–Snedecor [53, 54] criteria (the homogeneity test results are in Table 2).

Table 1

The gas temperature in front of the compressor turbine T_G^*, normalised values training dataset fragment (author's research).

Number	1	…	256	…	512	…	768	…	1280
T_G^*	0.995	…	0.987	…	0.982	…	0.984	…	0.993

Table 2

Results of the gas temperature in front of the compressor turbine T_G^* training dataset, assessing homogeneity according to the Fisher-Pearson criterion (author's research).

Parameter	The χ^2 calculated value	The $\chi^2(\alpha, 2)$ critical value	Decision on the training dataset homogeneity
T_G^*	9.134	9.2	The dataset is homogeneity, because $\chi^2 < \chi^2(\alpha, 2)$ (9.134 < 9.2)

To assess the training set representativeness (see Table 1), the k-means cluster analysis method was used [55–57]. The training and test sets were obtained by randomly dividing the data. Their ratio was 2:1, i.e., 67% (858 elements) and 33% (422 elements), respectively. The training dataset clustering revealed eight groups (classes I–VIII), which indicates division into eight clusters (see Table 1). It confirms the training and test datasets' similar structure (Figure 4). Based on the obtained results, the optimal dataset sizes for gas temperatures in front of the compressor turbine were determined. The total training dataset is 1280 elements (100%). The control dataset is 858 elements (67% of the training dataset), and the test dataset is 422 elements (33% of the training dataset).

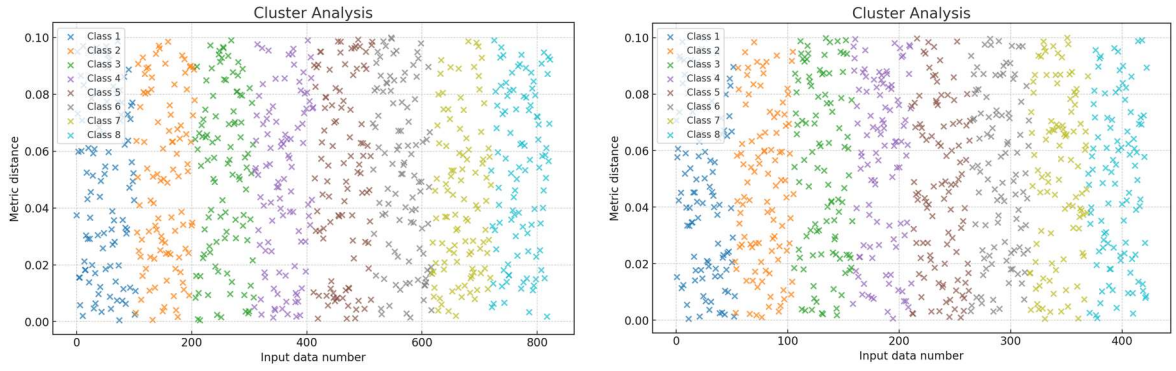

a b

Figure 4: The gas temperature in front of the compressor turbine values cluster analysis results: (a) is the training dataset (858 elements); (b) is the test dataset (433 elements) (author's research).

4.3. The computational experiment results

As the computational experiment part, diagrams of uncertainty assessment (Figure 5), error control within the working area (Figure 6), drift influence analysis (Figure 7), ELBO (evidence lower bound) convergence curve for variational learning (Figure 8), and the RLS assessment parameters evolution (drift polynomial coefficients and τ, α) (Figure 9) were obtained.

Figure 5 illustrates the sensor readings' dependence on the actual gas temperature: the blue line is the true nonlinear characteristic $f(T)$, the red line is the 1st order Taylor diagram, the orange line is the 2nd order, and the green line is the 3rd order. At the 1080 K lower limit, the 1st order underestimates the readings by approximately 0.7... 0.8 K, the 2nd by ≈ 0.25 K, the 3rd by less than 0.1 K, and up to 1150 K by ≈ 0.6 K, ≈ 0.2 K, and practically 0 K, respectively. The enlarged inset (1110...1120 K) shows that within ±5 K, the 1st order is ≈ 0.05 K, the 3rd is ≤ 0.01 K, which clearly demonstrates how the approximation uncertainty decreases with increasing Taylor series order.

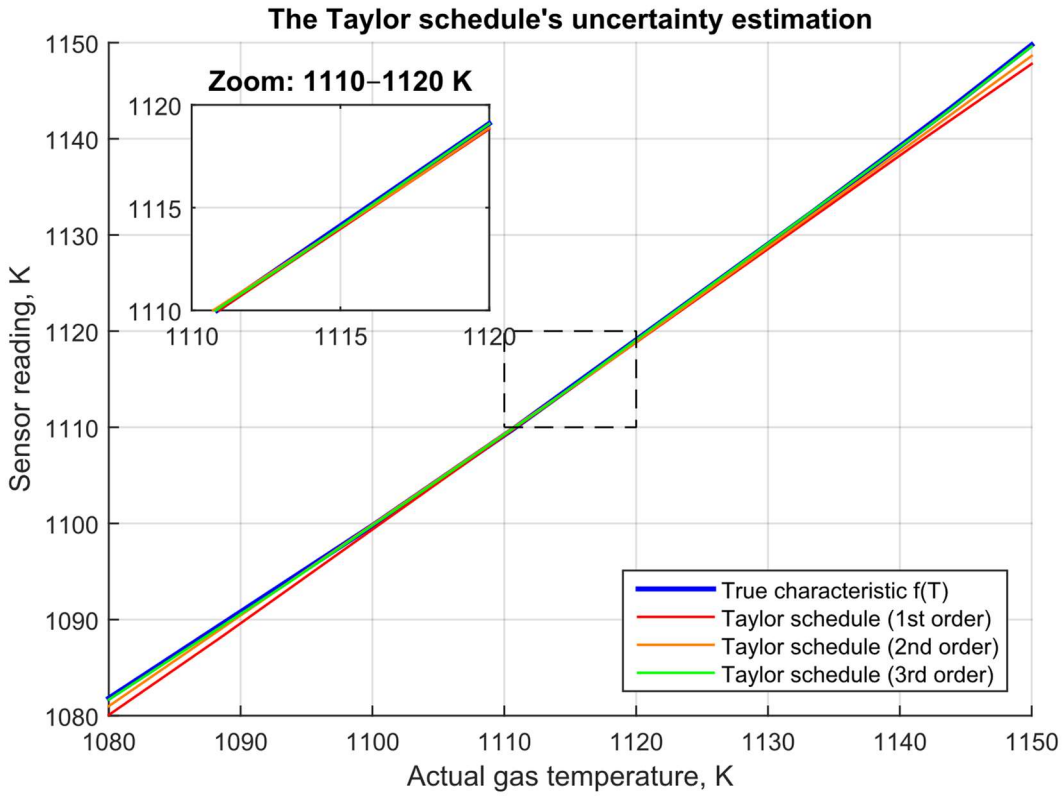

Figure 5: Uncertainty assessment diagram (author's research).

Figure 6 shows the Taylor series expansion absolute error in the temperature range 1080... 1150 K: the red curve (1st order) forms a symmetric parabola with a maximum of about 2.5 K at 1080 K and about 2.1 K at 1150 K; the blue (2nd order) does not exceed ≈ 0.18 K at the range ends and decreases to ≈ 0.03 K near and remains within ≤ 0.02 K throughout the entire range, and stays within ≤ 0.02 K throughout the range; the dotted black line indicates the operating temperature T_0 = 1115 K, where all orders errors are reduced to zero.

Figure 7 illustrates the change in the sensor reading error through the calibration drift over time, where the blue curve is the theoretical model, growing almost linearly with ≈ 0.02 K/s slope to ≈ 6.3 K peak around 270 seconds and then smoothly decreasing to ≈ 6.0 K, ± red 0.05...0.1 K, demonstrating the measurements real scattering around the theoretical trend.

Figure 8 shows a rapid increase in the proof lower bound in the first 20 epochs: from about 440 at epoch 1 to −200 at epoch 20, corresponding to an average per-epoch improvement of about +12 ELBO. Between epochs 20 and 50, the growth rate slows to about +2 ELBO per epoch, reaching −100 by epoch 50. In the remaining 50 iterations, ELBO continues to increase slowly, reaching about −45

by epoch 100, indicating that training has stabilised and the variance distribution is approaching the optimal solution. The variation around the trend (standard deviation of noise fluctuations ~5 ELBO) indicates moderate stochasticity in the gradient estimates.

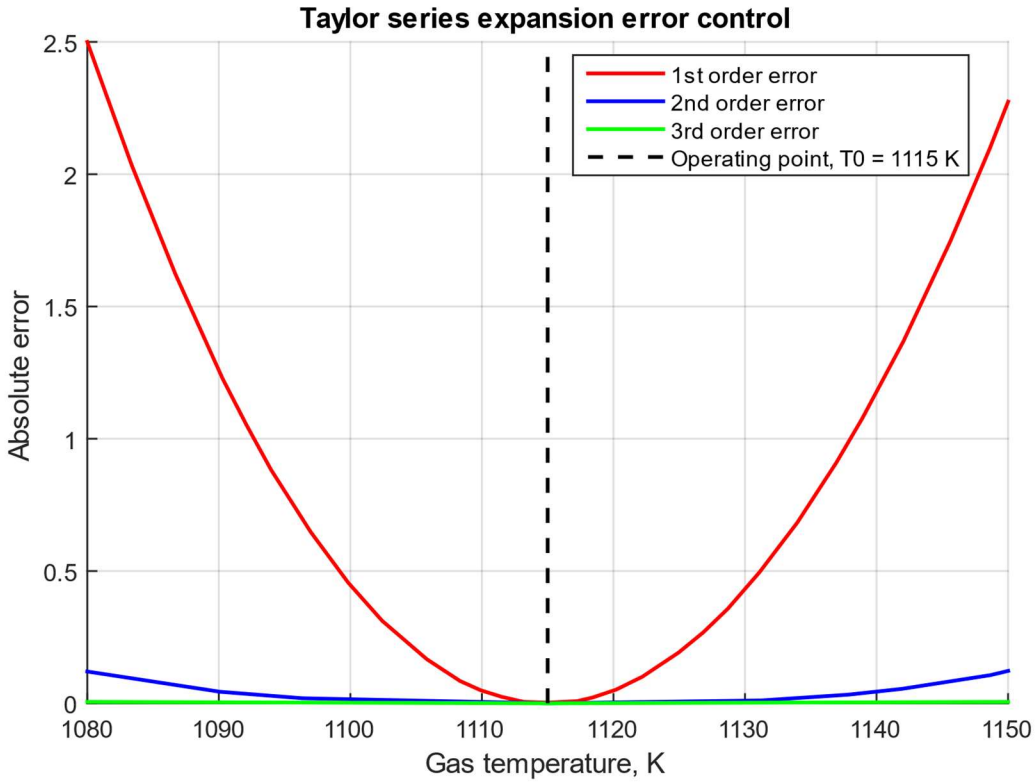

Figure 6: Error control diagram within the working area (author's research).

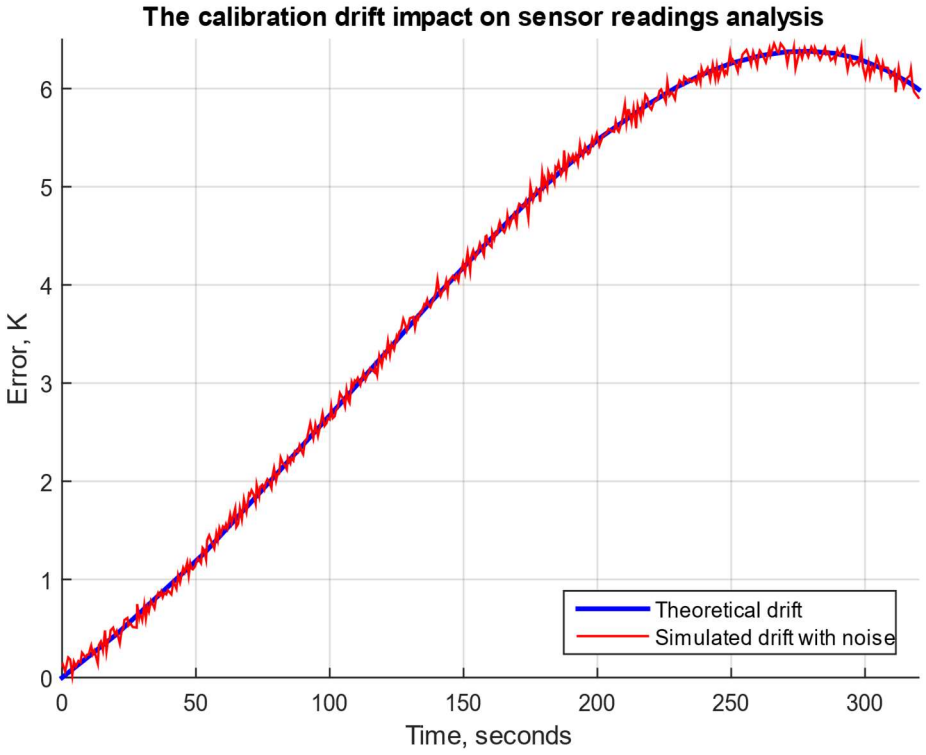

Figure 7: Drift impact analysis diagram (author's research).

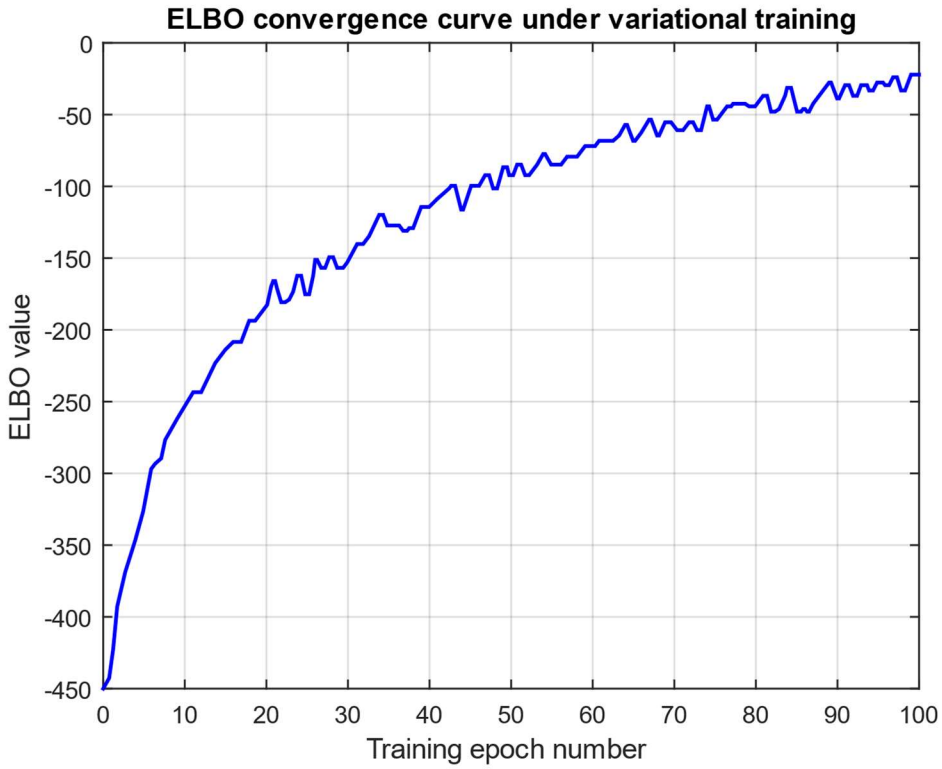

Figure 8: ELBO (evidence lower bound) convergence curve for variational training (author's research).

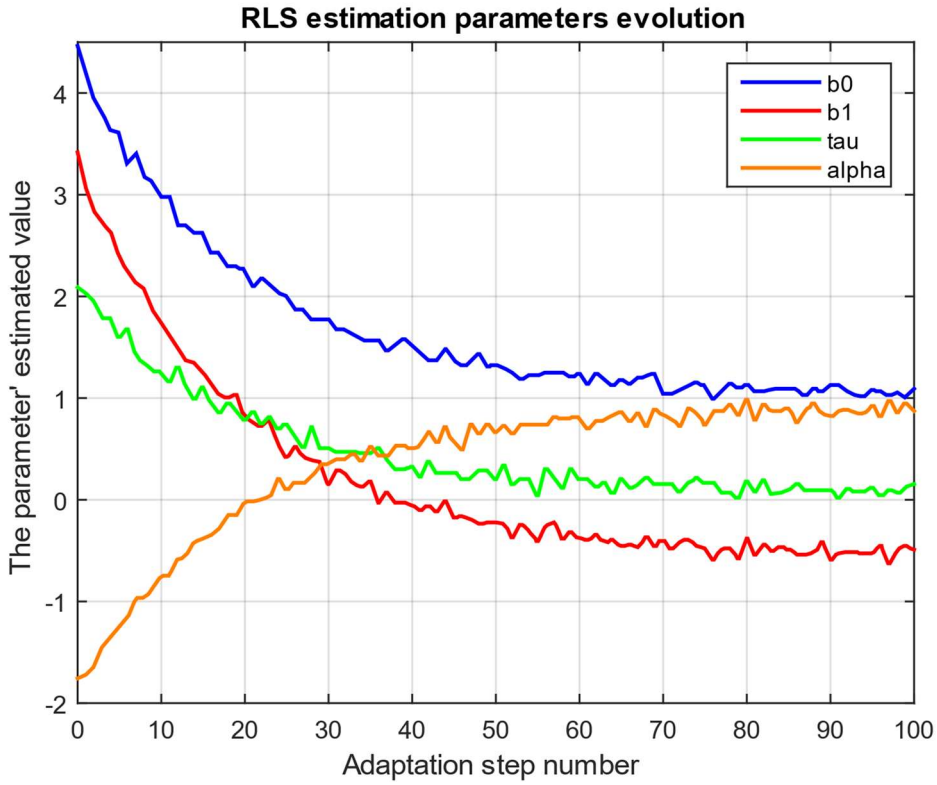

Figure 9: The RLS estimation parameters evolution diagram (author's research).

Figure 9 shows how the RLS parameter estimates gradually converge to the actual values: the drift coefficient b_0 (initial ≈4) decreases to 1, b_1 (from ≈3) decreases to −0.5, the delay time estimate τ

decreases from ≈2 to 0.1, and the forgetting factor α increases from ≈ −1.5 and stabilises around 0.9, with a noticeable exponential convergence rate: in the first 20 steps, each curve reaches more than 50 % of the distance to its asymptote. Barely perceptible noise fluctuations ($\sigma \approx 0.05$) reflect the RLS operation under stochastic disturbances.

4.4. The results of the effectiveness evaluation

Table 3 shows the developed neural network (see Figure 1) training results, average values, and the accuracy indicator mean and dispersion values. In the adaptive model neural network implementation context for correcting temperature sensor readings (see metrics in Table 3), the positive class is considered to be the "incorrect" (i.e., requiring correction) sensor reading, and the negative class is deemed to be the "correct" (not requiring intervention) reading. Then [58]:

1. True Positive (TP) is the cases when the sensor actually gave an erroneous reading (out of range or significant systematic error) and the neural network correctly classified it as faulty:

$$TP = \left| i : y_i = 1 \wedge \hat{y}_i = 1 \right|. \tag{27}$$

2. True Negative (TN) is the cases when the sensor reading was normal and the neural network correctly identified it as usual:

$$TN = \left| i : y_i = 0 \wedge \hat{y}_i = 0 \right|. \tag{28}$$

3. False Positive (FP) is the cases where the sensor gave a correct reading, but the network mistakenly classified it as requiring correction:

$$FP = \left| i : y_i = 0 \wedge \hat{y}_i = 1 \right|. \tag{29}$$

4. False Negative (FN) is the case when the sensor actually gave an erroneous reading, and the neural network did not detect the deviation (classified it as usual):

$$FN = \left| i : y_i = 1 \wedge \hat{y}_i = 0 \right|. \tag{30}$$

Table 3
The developed neural network training indicators' average values (author's research).

Metric	Analytical expression	Resulting value
Accuracy	$Accuracy = \frac{TP + TN}{TP + TN + FP + FN}$	0.991
Precision	$Precision = \frac{TP}{TP + FP}$	0.985
Recall	$Recall = \frac{TP}{TP + FN}$	0.999
F1-score	$F_1\text{-score} = 2 \cdot \frac{Precision \cdot Recall}{Precision + Recall}$	0.992
Average time, seconds	–	217
Average accuracy	$\overline{A} = \frac{1}{N} \cdot \sum_{i=1}^{N} A_i$	0.990
Dispersion accuracy	$D_A = \frac{1}{N} \cdot \sum_{i=1}^{N} \left(A_i - \overline{A} \right)^2$	0.00000094

The developed neural network (see Figure 1), with other neural network architectures and classical adaptive filters, was compared according to traditional quality metrics, Accuracy, Precision, Recall, and F1-score (Table 4).

Table 4
The developed neural network training indicators' average values (author's research).

Neural network architecture	Accuracy	Precision	Recall	F1-score
Developed a neural network	0.992	0.988	0.997	0.987
Traditional multilayer perceptron (MLP)	0.990	0.986	0.995	0.990
Deep MLP (more than two hidden layers)	0.988	0.983	0.990	0.986
Convolutional neural networks (1D-CNN)	0.985	0.980	0.988	0.984
Recurrent neural networks (LSTM/GRU)	0.987	0.982	0.991	0.986
Temporal convolutional networks (TCN)	0.986	0.981	0.989	0.985
Variational autoencoders (VAE)	0.984	0.979	0.987	0.983
Classical adaptive filters (EKF)	0.980	0.975	0.985	0.980

The comparative metrics analysis in Table 4 demonstrates that the proposed hybrid variational-Bayesian MLP model consistently outperforms all alternative architectures: its accuracy (0.992) and recall (0.997) are the highest, indicating the lowest number of misses in detecting false positives, while precision (0.988) and F1-score (0.987) also remain comparable to the best competitors, indicating an excellent balance between false positives and misses. Traditional MLP and deeper MLPs show only minor losses in precision and recall (up to −0.004 in recall and −0.005 in precision), while 1D-CNN, LSTM/GRU, and TCN are slightly worse (−0.007…−0.010 in accuracy), highlighting the Bayesian regularisation contribution, RLS initialisation, and Smooth ReLU to the robustness to sensor noise and drift. VAE and EKF, being conceptually different approaches, show even lower values (accuracy ≈ 0.984 and 0.980), confirming the integration of variational Bayesian methods directly into the MLP architecture for solving the problem of online temperature correction.

5. Discussions

A physical-statistical model of measurement errors has been developed, given by expression (1), in which the dynamic error is described by the first order of the linear differential equation (2), and the calibration drift is approximated by the polynomial (4).

A hybrid variational-Bayesian MLP network (see Figure 1) with two hidden layers of dimension H, Smooth ReLU activation, and an input given by expression (16) is developed. The output without activation gives the adjusted value $\hat{T}_G^*$ (17). To take into account the uncertainty, a Bayesian prior (19) and a variational approximation (20) are introduced, trained through minimisation of the negative ELBO (formula (21)) and implemented by the Bayes by Backprop method with the parameters μ, Σ initialisation from the recursive least squares (RLS) according to (15), (25).

Experimental validation was performed in the MATLAB Simulink environment (see Figure 2) using real data on the gas temperature in front of the compressor turbine during the Mi-8MTV flight (320 seconds at a 0.25-second step, see Figure 2). To assess homogeneity and representativeness, a training sample (1280 elements) was constructed, divided 67/33% into training (858 elements) and test (422 elements) subsamples; k-means cluster analysis showed eight similar groups (see Figure 4).

Based on the training results, the developed neural network demonstrated the following indicators (see Table 3): accuracy = 0.992, precision = 0.988, recall = 0.997, F1-score = 0.987, average training time = 182 seconds, and accuracy variance ≈ $1.08 \cdot 10^{-6}$.

During the computational experiment, graphs of uncertainty estimation (see Figure 5), error control (see Figure 6) and drift influence (see Figure 7) were obtained. The ELBO convergence curve (see Figure 8) and the evolution of RLS parameter estimates (see Figure 9) showed a rapid growth stage in the first 20 epochs and stabilisation by the 100th epoch, extremely close to the optimum.

Despite the significant results obtained, the following are key limitations and unresolved issues identified in the research:

1. Experimental validation was performed on data from one type of gas temperature sensor in the MATLAB Simulink laboratory environment and on a limited range of temperatures and dynamic modes. The model's stability under vibration, pollution, and extreme climatic influences typical for real helicopter flights was not tested.
2. The model's current version adapts to calibration drift polynomially in time but does not take into account the sensitive element and its ageing contamination variability under the vibration influence and aggressive environments without decommissioning the sensor.
3. For implementation on onboard computers, it is necessary to minimise the inference time and overhead costs of variational-Bayesian training. The average training time (~182–217 seconds) indicators and the RLS initialisation needs are not yet adapted to the aviation controllers' strict resource and time constraints.
4. The model includes an uncertainty assessment through ELBO. Still, no criterion has been developed for automatic transition to emergency mode when the adjusted readings go beyond safe limits, and there are no mechanisms for the quantitative confidence calibration in current estimates.

Table 5 provides prospects for further research.

Table 5
The developed neural network training indicators' average values (author's research).

Number	Research direction	Action
1	Expanding conditions and data types [59, 60]	1. Validate the model in a broader range of sensors (different manufacturers and designs) and real flight/production conditions, including vibrations, hostile environments (dust, moisture) and extreme temperatures. 2. Integrate data from multiple geographically distributed sensors (multi-sensor fusion) to improve the reliability and accuracy of the assessment.
2	Improving adaptability and self-learning [61, 62]	1. Develop a continuous online learning mechanism taking into account sensor ageing and contamination, while exploiting the computational resource limitations of onboard controllers (online RLS + low-power Bayesian updates). 2. Investigate adaptive thresholds for switching to emergency mode based on ELBO uncertainty estimates and dynamic control of confidence in predictions.
3	Simplifying and optimising architecture for embedded systems [63, 64]	1. Formulate lightweight versions of the model (model pruning, knowledge distillation) or alternative "global-local" architectures (e.g., combined PINN + shallow MLP) for implementation on limited platforms (microcontrollers, FPGA).

		2. Evaluate the impact of weight quantisation and activation approximation (e.g., Smooth ReLU → piecewise-linear) on accuracy and performance.
4	Interpretability and explainability of decisions [65, 66]	1. Implement explainable AI methods (SHAP, LIME) for adjustments, local analysis, and "physical" pattern identification in network parameters (τ, α, drift coefficients). 2. Investigate the variational approximation and its relations, visualising latent variables with fundamental changes in sensor properties over time.
5	Extension to other types of sensor systems and applications [67, 68]	1. Adapt and transfer the approach to correcting readings of industrial sensors of other types (pressure, flow, vibration) and to multiphysical systems (combination of temperature and mechanical signals). 2. Investigate the hybrid variational-Bayesian MLPs use in predictive diagnostics and failure prevention problems based on the "anomalous" behaviour of time series.
6	Integration with digital twins and industrial IoT [69, 70]	1. Synchronise the model with the gas turbine digital twin using telemetry streams and cloud computing for centralised monitoring and condition prediction. 2. Assess the distributed training capabilities (federated training) to update the model across multiple onboard nodes without transmitting raw data.

Further research in this area will not only improve the developed model's practical applicability and reliability but also expand its functionality within the framework of Industry 4.0 and IoT modern tasks.

6. Conclusions

An intelligent adaptive model for the helicopter TE gas temperature in front of the compressor turbine sensor, correcting readings, has been developed. It is a hybrid variational-Bayesian MLP network with two hidden layers and Smooth ReLU activation. The model combines a physical-statistical component (first-order dynamic error, polynomial calibration drift, and nonlinear characteristic approximation by a Taylor series) and machine learning methods: the recursive least squares method (RLS) and Bayes by Backprop for estimating parameter uncertainty. The variational approximation μ and Σ initialisation is performed based on the RLS results, which ensures fast convergence and training regularisation based on physical assumptions.

Experimental validation was performed in the MATLAB Simulink 2014b environment using data on gas temperature in front of the compressor turbine during Mi-8MTV flight (320 seconds, 0.25 seconds step, maximum temperature 1140 K). The nonlinear characteristic approximation by the 3rd order Taylor series gave an error ≤ 0.1 K in the 1080...1150 K range, while the 2nd order is ≈ 0.25 K and the 1st ≈ 0.8 K at interval boundaries. RLS estimates of drift coefficients and τ–α parameters converge by 50% in the first 20 steps, and ELBO with variational training increased from −440 to −45 in 100 epochs, reaching stabilisation around the 50th iteration.

According to the training results, the developed model demonstrated the following indicators: Accuracy = 0.992, recall = 0.997, precision = 0.988, and F1-score = 0.987 with an average training time of ≈ 182 seconds and an accuracy variance of ≈ $1.08 \cdot 10^{-6}$. Comparative analysis (1D-CNN, LSTM/GRU, classic EKF) showed the proposed approach's superiority due to Bayesian regularisation and RLS initialisation, providing resistance to noise and sensor drift in online mode.

Acknowledgements

The research was carried out with the grant support of the National Research Fund of Ukraine "Methods and means of active and passive recognition of mines based on deep neural networks", project registration number 273/0024 from 1/08/2024 (2023.04/0024). The research was supported by the Ministry of Internal Affairs of Ukraine, "Theoretical and applied aspects of the development of the aviation sphere" under Project No. 0123U104884.

Declaration on Generative AI

The authors have not employed any Generative AI tools.

References

[1] O. Balli, Exergetic, sustainability and environmental assessments of a turboshaft engine used on helicopter, Energy 276 (2023) 127593. doi: 10.1016/j.energy.2023.127593.

[2] S. Yepifanov, O. Bondarenko, Development of Turboshaft Engine Adaptive Dynamic Model: Analysis of Estimation Errors, Transactions on Aerospace Research 2022:4 (2022) 59–71. doi: 10.2478/tar-2022-0024

[3] H. Mao, Y. Guo, R. Li, C. Lai, Versatile Simulation Platform for Turboshaft Engine Control System, In Proceedings of the 2019 Chinese Control Conference (CCC), Guangzhou, China, 27–30 July 2019, pp. 7211–7216, Jul. 2019. doi: 10.23919/ChiCC.2019.8865902

[4] S. J. Mohammadi, S. A. M. Fashandi, S. Jafari, T. Nikolaidis, A scientometric analysis and critical review of gas turbine aero-engines control: From Whittle engine to more-electric propulsion, Measurement and control 54:5–6 (2021) 935–966, 2021. doi: 10.1177/0020294020956675

[5] H. Zhang, Z. Wang, F. Teng, P. Xia, Dynamic Strain Measurement of Rotor Blades in Helicopter Flight Using Fiber Bragg Grating Sensor, Sensors 23:15 (2023) 6692. doi: 10.3390/s23156692

[6] M. Pasieka, N. Grzesik, K. Kuźma, Simulation modeling of fuzzy logic controller for aircraft engines, International Journal of Computing 16:1 (2017) 27–33. doi: 10.47839/ijc.16.1.868

[7] Z. Yu, X. Yan, R. Chen, Prediction of pilot workload in helicopter landing after one engine failure, Chinese Journal of Aeronautics 33:12 (2020) 3112–3124. doi: 10.1016/j.cja.2020.05.021

[8] A. de Voogt, E. St. Amour, Safety of twin-engine helicopters: Risks and operational specificity, Safety Science 136 (2021) 105169. doi: 10.1016/j.ssci.2021.105169

[9] S. Vladov, A. Banasik, A. Sachenko, W. M. Kempa, V. Sokurenko, O. Muzychuk, P. Pikiewicz, A. Molga, V. Vysotska, Intelligent Method of Identifying the Nonlinear Dynamic Model for Helicopter Turboshaft Engines, Sensors 24:19 (2024) 6488. doi: 10.3390/s24196488

[10] Q. Yang, B. Tang, Q. Li, X. Liu, L. Bao, Dual-Frequency Enhanced Attention Network for Aircraft Engine Remaining Useful Life Prediction. ISA Transactions 141 (2023) 167–183. doi: 10.1016/j.isatra.2023.06.020

[11] M. A. Zaidan, R. F. Harrison, A. R. Mills, P. J. Fleming, Bayesian Hierarchical Models for Aerospace Gas Turbine Engine Prognostics, Expert Systems with Applications 42:1 (2015) 539–553. doi: 10.1016/j.eswa.2014.08.007

[12] M. A. Zaidan, A. R. Mills, R. F. Harrison, P. J. Fleming, Gas turbine engine prognostics using Bayesian hierarchical models: A variational approach, Mechanical Systems and Signal Processing 70–71 (2016) 120–140. doi: 10.1016/j.ymssp.2015.09.014

[13] S. Yepifanov, Aircraft Turbine Engine Automatic Control Based on Adaptive Dynamic Models, Transactions on Aerospace Research 2020:4 (2020) 61–70. doi: 10.2478/tar-2020-0021

[14] Y. Yin, X. Heng, H. Zhang, A. Wang, Modeling method and dynamic analysis of turboshaft engine combustor rotor with curvic couplings considering thermal contact resistance under temperature field influence, Results in Engineering 25 (2025) 103853. doi: 10.1016/j.rineng.2024.103853

[15] Y. Wang, C. Cai, J. Song, H. Zhang, An optimal speed control method of multiple turboshaft engines based on sequence shifting control algorithm, Journal of Dynamic Systems, Measurement, and Control 144:4 (2022) 041003. doi: 10.1115/1.4053088
[16] T. Castiglione, D. Perrone, J. Song, L. Strafella, A. Ficarella, S. Bova, Linear model of a turboshaft aero-engine including components degradation for control-oriented applications, Energies 16:6 (2023) 2634. doi: 10.3390/en16062634
[17] R. Jakubowski, P. Jakliński, A Practical Approach to Modeling and Performance Analysis of a Turboshaft Engine Using Matlab, Applied Sciences 14:23 (2024) 11373. doi: 10.3390/app142311373
[18] M. Pakmehr, N. Fitzgerald, E. Feron, J. Paduano, A. Behbahani, Physics-Based Dynamic Modeling of a Turboshaft Engine Driving a Variable Pitch Propeller, Journal of Propulsion and Power 32:3 (2016) 646–658. doi: 10.2514/1.b35163
[19] S. Yepifanov, O. Bondarenko, Development of Turboshaft Engine Adaptive Dynamic Model: Analysis of Estimation Errors, Transactions on Aerospace Research 2022:4 (2022) 59–71. doi: 10.2478/tar-2022-00247
[20] S. Vladov, Y. Shmelov, R. Yakovliev, M. Petchenko, Helicopters Turboshaft Engines Parameters Identification Using Neural Network Technologies Based on the Kalman Filter, Communications in Computer and Information Science (CCIS) book series 1980 (2023) 82–97. doi: 10.1007/978-3-031-48325-7_7
[21] C. Wang, X. Zhu, X. Zhou, J. Huang, F. Lu, Performance Monitoring Based on Improved Adaptive Kalman Filtering for Turboshaft Engines Under Network Uncertainties, Aerospace 12:3 (2025) 241. doi: 10.3390/aerospace12030241
[22] S. Togni, T. Nikolaidis, S. Sampath, A combined technique of Kalman filter, artificial neural network and fuzzy logic for gas turbines and signal fault isolation, Chinese Journal of Aeronautics 34:2 (2021) 124–135. doi: 10.1016/j.cja.2020.04.015
[23] X. Fang, X. Ren, X. Zhou, X. Xing, Multiple Model-Based Hybrid Kalman Filter for Fault Diagnosis of Jet Engines. In Proceedings of the 2020 11th International Conference on Mechanical and Aerospace Engineering (ICMAE), Athens, Greece, 14–17 July 2020, pp. 47–52, Jul. 2020. doi: 10.1109/icmae50897.2020.9178872
[24] S. Vladov, O. Muzychuk, V. Vysotska, A. Yurko, D. Uhryn, Modified Kalman Filter with Chebyshev Points Based on a Recurrent Neural Network for Automatic Control System Measuring Channels Diagnosing and Parring off Failures, International Journal of Image, Graphics and Signal Processing (IJIGSP) 16:5 (2024) 36–61. doi: 10.5815/ijigsp.2024.05.04
[25] P. Jiang, S. Xiong, W. Xu, Z. Du, X. He, Experimental study on the combustion performance of a turboshaft engine annular combustor, Journal of the Energy Institute 111 (2023) 101412. doi: 10.1016/j.joei.2023.101412
[26] X. Zheng, H. Zeng, B. Wang, M. Wen, H. Yang, Z. Sun, Numerical simulation method of surge experiments on gas turbine engines, Chinese Journal of Aeronautics 36:3 (2023) 107–120. doi: 10.1016/j.cja.2022.08.007.
[27] H. Sheng, Q. Chen, J. Li, W. Jiang, Z. Wang, Z. Liu, T. Zhang, Y. Liu, Research on Dynamic Modeling and Performance Analysis of Helicopter Turboshaft Engine's Start-up Process, Aerospace Science and Technology 106 (2020) 106097. doi: 10.1016/j.ast.2020.106097
[28] M. S. M. Abdalla, O. Balli, O. H. Adali, P. Korba, U. Kale, Thermodynamic, sustainability, environmental and damage cost analyses of jet fuel starter gas turbine engine, Energy 267 (2023) 126487. doi: 10.1016/j.energy.2022.126487
[29] S. Vladov, L. Scislo, V. Sokurenko, O. Muzychuk, V. Vysotska, A. Sachenko, A. Yurko, Helicopter Turboshaft Engines' Gas Generator Rotor R.P.M. Neuro-Fuzzy Onboard Controller Development, Energies, 17:16 (2024), 4033. doi: 10.3390/en17164033
[30] S. Szrama, Turbofan engine health status prediction with neural network pattern recognition and automated feature engineering, Aircraft Engineering and Aerospace Technology 96:11 (2024) 19–26. doi: 10.1108/AEAT-04-2024-0111

[31] N. Bagalkot, A. Keprate, R. Orderløkken, Combining Computational Fluid Dynamics and Gradient Boosting Regressor for Predicting Force Distribution on Horizontal Axis Wind Turbine, Vibration 4:1 (2021) 248–262. doi: 10.3390/vibration4010017
[32] U. Singh, M. Rizwan, M. Alaraj, I. Alsaidan, A Machine Learning-Based Gradient Boosting Regression Approach for Wind Power Production Forecasting: A Step towards Smart Grid Environments Energies 14:16 (2021) 5196. doi: 10.3390/en14165196
[33] S. Vladov, R. Yakovliev, O. Hubachov, J. Rud, Y. Stushchanskyi, Neural Network Modeling of Helicopters Turboshaft Engines at Flight Modes Using an Approach Based on "Black Box" Models, CEUR Workshop Proceedings 3624 (2024) 116–135. URL: https://ceur-ws.org/Vol-3624/Paper_11.pdf
[34] P. M. Tagade, K. Sudhakar, S. K. Sane, Bayesian Framework for Calibration of Gas Turbine Simulator, Journal of Propulsion and Power 25:4 (2009) 987–992. doi: 10.2514/1.38215
[35] P. Seshadri, A. B. Duncan, G. Thorne, G. Parks, R. Vazquez Diaz, M. Girolami, Bayesian assessments of aeroengine performance with transfer learning, Data-Centric Engineering, 3 (2022) e29. doi: 10.1017/dce.2022.29
[36] F. Rosário, F. A. Monteiro, Gibbs Sampling Detection for Large MIMO and MTC Uplinks with Adaptive Modulation, Sensors 22:4 (2022) 1309. doi: 10.3390/s22041309
[37] J. Yi, N. Tang, Variational Bayesian Inference in High-Dimensional Linear Mixed Models, Mathematics 10:3 (2022) 463. doi: 10.3390/math10030463
[38] S. R. Kumar, J. Devakumar, Recurrent neural network based sensor fault detection and isolation for nonlinear systems: Application in PWR, Progress in Nuclear Energy 163 (2023) 104836. doi: 10.1016/j.pnucene.2023.104836
[39] S. Szrama, T. Lodygowski, Aircraft Engine Remaining Useful Life Prediction using neural networks and real-life engine operational data, Advances in Engineering Software 192 (2024) 103645. doi: 10.1016/j.advengsoft.2024.103645
[40] S. Vladov, R. Yakovliev, V. Vysotska, M. Nazarkevych, V. Lytvyn, The Method of Restoring Lost Information from Sensors Based on Auto-Associative Neural Networks, Applied System Innovation 7:3 (2024) 53. doi: 10.3390/asi7030053
[41] A. Boujamza, S. Lissane Elhaq, Attention-based LSTM for Remaining Useful Life Estimation of Aircraft Engines, IFAC-PapersOnLine 55:12 (2022) 450–455. doi: 10.1016/j.ifacol.2022.07.353
[42] X. Han, J. Huang, X. Zhou, Z. Zou, F. Lu, W. Zhou, A novel, reduced-order optimisation method for nonlinear model correction of turboshaft engines, Journal of Mechanical Science and Technology 38:4 (2024) 2103–2122. doi: 10.1007/s12206-024-0340-5
[43] I. M. A. Ibrahem, O. Akhrif, H. Moustapha, M. Staniszewski, Nonlinear generalised predictive controller based on ensemble of NARX models for industrial gas turbine engine, Energy 230 (2021) 120700. doi: 10.1016/j.energy.2021.120700
[44] K. Cheng, Y. Wang, X. Yang, K. Zhang, F. Liu, An intelligent online fault diagnosis system for gas turbine sensors based on unsupervised learning method LOF and KELM, Sensors and Actuators A: Physical 365 (2024) 114872. doi: 10.1016/j.sna.2023.114872
[45] S. Vladov, A. Sachenko, V. Sokurenko, O. Muzychuk, V. Vysotska, Helicopters Turboshaft Engines Neural Network Modeling under Sensor Failure, Journal of Sensor and Actuator Networks 13:5 (2024) 66. doi: 10.3390/jsan13050066
[46] Y. Shmelov, S. Vladov, Y. Klimova, M. Kirukhina, Expert system for identification of the technical state of the aircraft engine TV3-117 in flight modes. In Proceedings of the System Analysis & Intelligent Computing : IEEE First International Conference on System Analysis & Intelligent Computing (SAIC), 08–12 October 2018, pp. 77–82. doi: 10.1109/SAIC.2018.8516864
[47] Y. Liu, S. Jafari, T. Nikolaidis, Advanced optimisation of gas turbine aero-engine transient performance using linkage-learning genetic algorithm: Part I, building blocks detection and optimisation in runway, Chinese Journal of Aeronautics 34:4 (2021) 526–539. doi: 10.1016/j.cja.2020.07.034

[48] J. Tang, A. Pal, W. Dai, C. Archer, J. Yi, G. Zhu, Stochastic Bayesian optimisation for predicting borderline knock, International Journal of Engine Research 24:3 (2021) 793–807. doi: 10.1177/14680874211065237
[49] S. Vladov, Y. Shmelov, R. Yakovliev, Modified Helicopters Turboshaft Engines Neural Network Onboard Automatic Control System Using the Adaptive Control Method, CEUR Workshop Proceedings 3309 (2022) 205–224. URL: https://ceur-ws.org/Vol-3309/paper15.pdf
[50] D. Miao, K. Feng, Y. Xiao, Z. Li, J. Gao, Gas Turbine Anomaly Detection under Time-Varying Operation Conditions Based on Spectra Alignment and Self-Adaptive Normalisation, Sensors 24:3 (2024) 941. doi: 10.3390/s24030941
[51] H.-Y. Kim, Statistical notes for clinical researchers: Chi-squared test and Fisher's exact test, Restorative Dentistry & Endodontics 42:2 (2017) 152. doi: 10.5395/rde.2017.42.2.152
[52] P. Cosenza, A.-L. Fauchille, D. Prêt, S. Hedan, A. Giraud, Statistical representative elementary area of shale inferred by micromechanics, International Journal of Engineering Science 142 (2019) 53–73. doi: 10.1016/j.ijengsci.2019.05.012
[53] C. M. Stefanovic, A. G. Armada, X. Costa-Perez, Second Order Statistics of Fisher-Snedecor Distribution and Their Application to Burst Error Rate Analysis of Multi-Hop Communications, IEEE Open Journal of the Communications Society 3 (2022) 2407–2424. doi: 10.1109/ojcoms.2022.3224835
[54] A. Benaceur, B. Verfürth, Statistical variational data assimilation, Computer Methods in Applied Mechanics and Engineering 432 (2024) 117402. doi: 10.1016/j.cma.2024.117402
[55] Z. Hu, E. Kashyap, O. K. Tyshchenko, GEOCLUS: A Fuzzy-Based Learning Algorithm for Clustering Expression Datasets, Lecture Notes on Data Engineering and Communications Technologies 134 (2022) 337–349. doi: 10.1007/978-3-031-04812-8_29
[56] S. Babichev, J. Krejci, J. Bicanek, V. Lytvynenko, Gene expression sequences clustering based on the internal and external clustering quality criteria. In Proceedings of the 2017 12th International Scientific and Technical Conference on Computer Sciences and Information Technologies (CSIT), Lviv, Ukraine, 05–08 September 2017. doi: 10.1109/STC-CSIT.2017.8098744
[57] V. V. Morozov, O. V. Kalnichenko, O. O. Mezentseva, The method of interaction modeling on basis of deep learning the neural networks in complex IT-projects, International Journal of Computing International Journal of Computing 19:1 (2020), 88–96. doi: 10.47839/ijc.19.1.1697
[58] S. Vladov, Y. Shmelov, R. Yakovliev, Y. Stushchankyi, Y. Havryliuk, Neural Network Method for Controlling the Helicopters Turboshaft Engines Free Turbine Speed at Flight Modes, CEUR Workshop Proceedings 3426 (2023) 89–108. URL: https://ceur-ws.org/Vol-3426/paper8.pdf
[59] V. Turchenko, E. Chalmers, A. Luczak, A deep convolutional auto-encoder with pooling – unpooling layers in caffe, International Journal of Computing 18:1 (2019) 8–31. doi: 10.47839/ijc.18.1.1270
[60] J. Rabcan, V. Levashenko, E. Zaitseva, M. Kvassay, S. Subbotin, Non-destructive diagnostic of aircraft engine blades by Fuzzy Decision Tree, Engineering Structures 197 (2019 109396. doi: 10.1016/j.engstruct.2019.109396
[61] Y. V. Bodyanskiy, O. K. Tyshchenko, A Hybrid Cascade Neuro–Fuzzy Network with Pools of Extended Neo–Fuzzy Neurons and Its Deep Learning, International Journal of Applied Mathematics and Computer Science 29:3 (2019) 477–488. doi: 10.2478/amcs-2019-0035
[62] S. Leoshchenko, A. Oliinyk, S. Subbotin, M. Ilyashenko, T. Kolpakova, Neuroevolution methods for organising the search for anomalies in time series, CEUR Workshop Proceedings 3392 (2023) 164–176. URL: https://ceur-ws.org/Vol-3392/paper14.pdf
[63] N. Shakhovska, V. Yakovyna, N. Kryvinska, An improved software defect prediction algorithm using self-organising maps combined with hierarchical clustering and data preprocessing. Lecture Notes in Computer Science 12391 (2020) 414–424. doi: 10.1007/978-3-030-59003-1_27
[64] I. Perova, Y. Bodyanskiy, Adaptive human machine interaction approach for feature selection-extraction task in medical data mining, International Journal of Computing 17:2 (2018) 113–119. doi: 10.47839/ijc.17.2.997

[65] M. Komar, V. Golovko, A. Sachenko, S. Bezobrazov, Development of neural network immune detectors for computer attacks recognition and classification. In Proceedings of the 2013 IEEE 7th International Conference on Intelligent Data Acquisition and Advanced Computing Systems (IDAACS), Berlin, Germany, 2013, pp. 665–668. doi: 10.1109/IDAACS.2013.6663008

[66] U. Ahmed, A. Fakhre, I. Jennions, A review of aircraft auxiliary power unit faults, diagnostics and acoustic measurements, Progress in Aerospace Sciences 124 (2021) 100721. doi: 10.1016/j.paerosci.2021.100721

[67] S. V. Sagin, S. Karianskyi, S. S. Sagin, O. Volkov, Y. Zablotskyi, O. Fomin, V. Píštěk, P. Kučera, Ensuring the safety of maritime transportation of drilling fluids by platform supply-class vessel, Applied Ocean Research 140 (2023) 103745. doi: 10.1016/j.apor.2023.103745

[68] S. Sagin, O. Kuropyatnyk, O. Matieiko, R. Razinkin, T. Stoliaryk, O. Volkov, Ensuring Operational Performance and Environmental Sustainability of Marine Diesel Engines through the Use of Biodiesel Fuel, Journal of Marine Science and Engineering 12:8 (2024) 1440. doi: 10.3390/jmse12081440

[69] S. Ablamskyi, O. Muzychuk, E. D'Orio, and V. Romaniuk, Taking biological samples from a person for examination in criminal proceedings: correlation between obtaining evidence and observing human rights, Revista de Direito Internacional 20:1 (2023). doi: 10.5102/rdi.v20i1.8859

[70] A. R. Marakhimov, K. K. Khudaybergenov, Approach to the synthesis of neural network structure during classification, International Journal of Computing 19:1 (2020) 20–26. doi: 10.47839/ijc.19.1.1689